SCIENCE CHINA
Information Sciences

• RESEARCH PAPER •

October 2024, Vol. 67, Iss. 10, 202202:1–202202:17
https://doi.org/10.1007/s11432-023-4015-1

Adaptive coupled-sliding-variable-based finite-time control of composite formation for multi-robot systems

Xinru MA[1], Hengyu LI[1*], Jun LIU[2], Yueying WANG[1], Shaorong XIE[1,3] & Jun LUO[4]

[1]*School of Mechatronic Engineering and Automation, Shanghai University, Shanghai* 200444*, China;*
[2]*School of Mathematics and Computer Application Technology, Jining University, Qufu* 273155*, China;*
[3]*School of Computer Science, Shanghai University, Shanghai* 200444*, China;*
[4]*College of Mechanical and Vehicle Engineering, Chongqing University, Chongqing* 400030*, China*

Received 27 April 2023/Revised 27 July 2023/Accepted 19 September 2023/Published online 26 September 2024

Abstract This paper focuses on the finite-time control (FTC) of the composite formation consensus (CFC) problems for multi-robot systems (MRSs). The CFC problems are firstly proposed for MRSs under the complex network topology of cooperative or cooperative-competitive networks. Regarding the problems of FTC and CFC on multiple Lagrange systems (MLSs), coupled sliding variables are introduced to deal with the robustness and consistent convergence. Then, the adaptive finite-time protocols are given based on the displacement approaches. With the premised FTC, tender-tracking methods are further developed for the problems of tracking information disparity. Stability analyses of those MLSs mentioned above are clarified with Lyapunov candidates considering the coupled sliding vectors, which provide new verification for tender-tracking systems. Under the given coupled-sliding-variable-based finite-time protocols, MLSs distributively adjust the local formation error to achieve global CFC and perform uniform convergence in time-varying tracking. Finally, simulation experiments are conducted while providing practical solutions for the theoretical results.

Keywords composite formation, time-vary tracking, information disparity, tender-tracking, finite-time control, nonlinear robots, complex networks, symmetry consensus

1 Introduction

The control theory of multi-agent systems (MASs) originated from the problems of composite assignments in complex environments. Based on the theoretical work of Olfati-Saber and Murray [1] and Ren and Beard [2], MAS consensus problems and the coordination of MASs are then established. The coordination of MASs is widely used in, for example, search and rescue in hazardous environments, detection of unknown environments, and communication over large spans. It is well known that multi-agent collaboration is realized with the support of algorithms that search for reachable communication networks. For example, Lu et al. [3] solved the dynamic collision avoidance problem for surface unmanned vehicles using a particle swarm optimization algorithm. The studies mentioned above occupy half of the research on cooperative control. The other half of the work in this area is the design of controllers for task objectives, focusing on compatibility with the dynamics and kinematics of the agents. It is noteworthy that the specified formation is essential for most of the composite assignments. For practical scenes, such as area coverage in military missions, sensing expansion of space satellite constellations, and throughput management for unmanned road transport, the desired formation of MASs is a major requirement of coordination. Therefore, formation control has been the most active research in MAS coordination. Moreover, formation consensus (FC) is necessary for formation control problems. As interaction topology and sensing capabilities are involved, the existing studies solve the FC problems through the location-based method, the displacement-based method, and the distance-based method. If MASs can determine the direction of the global coordinate system but are not informed about the global coordinates and are

* Corresponding author (email: lihengyu@shu.edu.cn)

unaware of the relative position to the global coordinate system, then, displacement-based methods are used to achieve FC. That means the displacement-based method enables MASs to be highly autonomous. This paper will also follow the displacement-based control method to solve the FC problems.

The simultaneous formation maintaining and movement are resorted as composite formation problems. For example, encircling and tracking targets require simultaneous formation keeping, formation tracking, and re-formation. Thus, the research work of MASs to achieve composite formation consensus (CFC) has been quested in various aspects. As one of the key aspects affecting control performance, the controllers' response rate has received attention. Based on the finite-time control framework given by Venkataraman et al. [4] and Bhat et al. [5], Xiao et al. [6] developed the formation framework of leader-global and leader-local under finite-time control for MASs with one-order linear dynamics; Li et al. [7] discussed the finite-time consensus problem for MASs with external disturbances and double-integrator dynamics; Zhao et al. [8] used a displacement-based approach to study the distributed finite-time tracking for second-order multi-agent systems. In this point, the system controllers' response rate is also the study's main object.

Overall, these aforementioned studies explore MASs described by general dynamics equations. In fact, in unmanned control engineering, the coordination researches of MASs composed of multiple unmanned road vehicles, multiple robots, or multiple unmanned ocean vehicles are much more interesting. Therefore, the coordination study of specific mechanical models has become a challenge work in recent years. Li et al. [9] solved the challenge of vehicular platoon stability using the predefined-time terminal sliding mode to deal with unknown nonlinear systems; Zhou et al. [10] investigated cooperative path tracking of unmanned surface vehicles based on a time-triggered approach with state constraints under improved communication rate requirements; Wu et al. [11] constructed a novel collision-free adaptive output-feedback controller for reaching FC of stochastic nonlinear MASs with immeasurable states; Cui et al. [12] proposed the state feedback and output feedback adaptive agent predefined-time control strategies for fractional-order nonlinear systems. Different from the aforementioned mechanical models, this paper will discuss multi-robot systems (MRSs), in which each robot has a nonlinear Lagrangian dynamical system.

Compared to the aforementioned second-order systems, robotic systems have higher manufacturability in engineering. The most important aspect of robot control is the mechanism of movement, which relies on analyzing the dynamics of the robot. The Lagrange dynamics equation contains the kinematic characteristics and dynamics of robotic systems such as manipulators and robotic arms. Therefore, using Lagrange dynamics equations to consider robot control can improve its action function and response performance. Various concrete entities such as ocean unmanned vehicles, flexible spacecraft, and manipulator arms are known as Lagrange robots. For instance, Wu et al. [13] studied event-triggered tracking control of surface vehicles, described by Lagrange dynamics equations. Moreover, as second-order systems, Lagrange robots integrate flexibility, mobility, and reliability. Therefore, the research on multiple Lagrange robot systems (MLSs) continues to be pushed to realize swarming intelligent robots. Liu and Zhou [14] worked on distributed swarming consensus for networked MLSs based on the impulse sampling protocols with acyclic partitioning topology, and further proposed the integral sliding mode controller for MLSs in the directed partitioned topology [15, 16]; Roy et al. [17] produced adaptive control algorithms for the robustness of networked MLSs in the presence of bounded uncertain parameters; Lu and Liu [18] studied the leader-follower consensus control problems for MLSs with uncertain parameters of leader dynamics; Ge et al. [19] used recursive controller-estimators to study the coordination problems of networked MLSs; Dong et al. [20] investigated fixed-time synchronization of MLSs using a distributed observer.

The above results show a large number of theoretical studies about the distributed consensus [14,15,17] and leader-follower consensus [18, 20] for MLSs with uncertain parameters. Many recent studies are also developed for distributed FC [21] and leader-follower-based FC [22, 23] of MLSs with uncertain parameters. Zhao et al. [24] investigated the distributed finite-time tracking protocols for MLSs; Sun et al. [22] provided finite-time protocols for the time-varying formation of MLSs; Yu et al. [21] researched distributed formation problems for parameters uncertain MLSs with collision avoidance; Zhou et al. [23] further investigated the formation containment problems for MLSs with unknown bounded inputs to the leader; Fan et al. [25] introduced observers of immeasurable velocities to solve the FC problems of MLSs through the super-twisting algorithm. Indeed, these studies can be further detected for finite-time control of MLSs. Although studies on finite-time control of MLSs exist [24, 25], these decouple MLSs into generalized second-order systems for study. That is, the inherent uncertainty of the Lagrange dynamics parameters is not concerned. As a mathematical model describing the state and motion of a robot, the Lagrange dynamics equation is a nonlinear model. With different states and external forces, there are

variations in robot parameters and coupling of state variables. Therefore, it is not possible to use only position closed-loop control as in a general nonlinear system. At this point, the robot control system also requires a velocity closed loop or even an acceleration closed loop. Because of these unique characteristics, the classical control theory and modern control theory cannot be copied and used. However, so far, the dynamics-based robot control theory and MLSs' coordination control theory are still incomplete and unsystematic. Ref. [22] ultimately solved the problem of formation control with uncertain parameters for MLSs in a leader-centralized way. This suggests that the finite-time distributed formation control problems for MLSs have not yet been solved. Therefore, this paper will study the CFC problems for MLSs.

In this paper, the first challenge is to solve the limitation of traditional finite-time control methods on nonlinear MLSs. And second, the finite-time protocols must consider parameter uncertainty. The main work is assigned to provide adaptive control protocols for these two challenges using sliding mode variables. In addition, the new CFC problems of FTC are further proposed with tender-tracking. The main contributions are listed below.

(1) This paper proposed a novel distributed finite-time formation protocol based on the introduced coupled sliding variables. The coupled sliding variables can accommodate the requirements of the torque controller for MLSs, thus solving the second-order nonlinear system characterized by parameter uncertainty of MLSs.

(2) It further formulated a formation tracking control by tender assignments. Through the tender approach, the MLS can realize flexible and variable CFC in finite time according to the tracking signals. The control method of tender tracking is more variable and programmable than the leader-centralized tracking method.

(3) The new analysis of systems is the layout for verifying the coupled-sliding-variable-based control and the tender-tracking protocols, which validate the above two methods. The critical approach is to analyze the system state variables using coupled sliding mode variables and derive the finite-time formation agreement and finite-time formation tracking for MLSs.

2 Preliminaries

This section includes graph theory, dynamics basics, nonlinear analysis, and problem formulation. Lagrange dynamics equations give explicit expressions of multiple robots with uncertain parameters. Note that this article will use a displacement-based method to realize formation control.

2.1 Graph topology

In this paper, the signed digraph $\mathcal{G} = (\mathcal{V}, \mathcal{E})$ will be considered. Let $\mathcal{V} = \{1, 2, \ldots, n\}$. Suppose that $\mathcal{E}$ is the edges set regarding the links between pair nodes. The real matrix $A = [a_{ij}]_{n\times n}$ is adjacency matrix of $\mathcal{G}$. The adjacency matrix of the digraph will not necessarily be symmetry. Moreover, $\left\{\mathcal{V}^{(1)}, \mathcal{V}^{(2)}\right\}$ is called one partition of $\mathcal{G}$ if $\mathcal{V}^{(1)} \cap \mathcal{V}^{(2)} = \emptyset$ and $\mathcal{V}^{(1)} \cup \mathcal{V}^{(2)} = \mathcal{V}$. Then graph $\mathcal{G}$ is structurally balance if and only if partition $\left\{\mathcal{V}^{(1)}, \mathcal{V}^{(2)}\right\}$ satisfies that $a_{ij} \leqslant 0$ for $i, j \in \mathcal{V}^{(1)}$ or $i, j \in \mathcal{V}^{(2)}$, and $a_{ij} \geqslant 0$ for $i \in \mathcal{V}^{(1)}$, $j \in \mathcal{V}^{(2)}$ [26]. This paper discusses graph topology that satisfies the following assumptions.

Assumption 1. $\mathcal{G}$ is structurally balance.

Along with Assumption 1, there is a diagonal matrix $\Phi = \operatorname{diag}\{\phi_1, \phi_2, \ldots, \phi_n\}$ with principle elements $\phi_i = 1$ or $\phi_i = -1$. Then matrix A can be transformed into $\Phi A \Phi$, which has non-negative entries [26]. In this point, the Laplace matrix $L = [l_{ij}]_{n\times n}$ of topology $\mathcal{G}$ is defined by $l_{ij} = -a_{ij}$ for $i \neq j$ and $l_{ii} = \sum_{j\in\mathcal{V}} |a_{ij}|$. As discussed before, $\Phi A \Phi$ is the adjacency matrix of a non-signed graph. Actually, the matrix Φ will be the identity matrix if $\mathcal{G}$ is the non-signed graph. Thus the networks discussed in this paper contain both complete and bipartite topology. Under the definition of the Laplace matrix, the equation $\Phi L(A)\Phi = L(\Phi A \Phi)$ holds, which ensures the bipartite consensus problems to be solved by solutions of complete consensus.

Assumption 2. $\mathcal{G}$ has a directed spanning tree.

With Assumption 1, $\Phi L \Phi$ has 1_n as right eigenvector of eigenvalue 0. Corresponding to Assumption 2, eigenvalue 0 is algebraically simple while other eigenvalues have positive real parts. And there exists

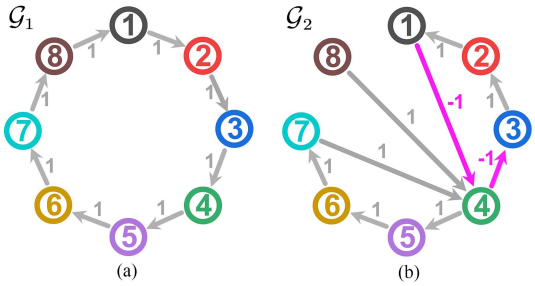

Figure 1 (Color online) (a) Non-bipartite topology: $\Phi_{\mathcal{G}_1} = \mathrm{diag}(1,1,1,1,1,1,1,1)$; (b) bipartite topology: $\Phi_{\mathcal{G}_2} = \mathrm{diag}(-1,-1,-1,1,1,1,1,1)$.

positive vector π such that $\pi^{\mathrm{T}}\Phi L\Phi = 0$ [14]. Let

$$\Psi_i = \begin{bmatrix} I_{i-1} & -\mathbf{1}_{i-1} & \mathbf{0} \\ & \pi^T & \\ \mathbf{0} & \mathbf{1}_{n-i} & -I_{n-i} \end{bmatrix}, \ i \in \mathcal{V}.$$

Each Ψ_i is, obviously, invariable. Under these two assumptions, one has

$$\Psi_i\Phi L(\Psi_i\Phi)^{-1} = \begin{bmatrix} L_{i_1} & \mathbf{0}^{\mathrm{T}} & L_{i_2} \\ \mathbf{0}^{\mathrm{T}} & 0 & \mathbf{0}^{\mathrm{T}} \\ L_{i_3} & \mathbf{0}^{\mathrm{T}} & L_{i_4} \end{bmatrix}, \tag{1}$$

where $\mathbf{0}$ is the vector with the appropriate order. Moreover, $\left[\begin{smallmatrix} L_{i_1} & L_{i_2} \\ L_{i_3} & L_{i_4} \end{smallmatrix}\right] \doteq L_i$ is Hurwitz matrix [2].

As is shown in Figure 1(a), $\mathcal{G}_1$ presents a non-signed graph. For comparison, Figure 1(b) presents a signed graph $\mathcal{G}_2$, which is bipartite about set $\{1,2,3\}$ and set $\{4,5,6,7,8\}$.

2.2 Lagrange dynamics

Letting $q(t) \in \mathbb{R}^p$ be generalized coordinate of one Lagrange robot, the kinetic coefficient matrices are the inertia matrix $M(q(t)) \in \mathbb{R}^{p\times p}$, the matrix $C(q(t),\dot{q}(t)) \in \mathbb{R}^{p\times p}$ of centrifugal and Coriolis forces, and the gravitational torque vector $g(q(t)) \in \mathbb{R}^p$. And the dynamics satisfies $M(q(t))\ddot{q}(t) + C(q(t),\dot{q}(t))\dot{q}(t) + g(q(t)) = \tau(t)$, where $\tau(t) \in \mathbb{R}^p$ is the control torque. In addition to that $M(q(t))$ is symmetric positive definite, it is needed to mention the properties for such a Lagrange system with uncertain parameters.

Lemma 1 ([27]). There exist positive constants b_M, B_M, B_C, and B_g for any vectors u, v in $\mathbb{R}^p$ such that $b_M I_p \leqslant M(q(t)) \leqslant B_M I_p$, $\|C(q(t),u)v\| < B_C\|u\|\|v\|$, and $\|g(q(t))\| < B_g$.

This boundedness property of dynamic coefficient matrices is an initial requirement concerning system load.

Lemma 2 ([27]). The matrix $\dot{M}(q(t)) - 2C(q(t),\dot{q}(t))$ is skew-symmetric.

The body of the Lagrange robot is featured by this property with generalized coordinate $q(t)$.

Lemma 3 ([27]). For one certain kinetic constant vector θ, the following equation holds for arbitrary differentiable vector $u, v \in \mathbb{R}^p$:

$$M(q(t))u + C(q(t),\dot{q}(t))v + g(q(t)) = Y(q(t),\dot{q}(t),u,v)\theta, \tag{2}$$

in which $Y(q(t),\dot{q}(t),u,v)$ is the regressive matrix relating θ.

In case of parametric uncertainty, the control methods also need to consider the uncertainty. Meanwhile, only the estimates of $M(q(t))$, $C(q(t),\dot{q}(t))$, $g(q(t))$ can be used to design the controller for the Lagrange robot. As Lemma 3 is given, the Lagrange dynamics equation is linear about its kinetic parameter. Thus, the control protocols can only consider estimates of parameter θ. Additionally, θ can be selected as the moment vector of a rigid body under the orthogonal basis.

As this article discusses multi-Lagrange systems under topology $\mathcal{G}$, let $q_i(t)$ denote the generalized coordination of robot i ($i \in \mathcal{V}$). Then MLSs have dynamics as

$$M_i(q_i(t))\ddot{q}_i(t) + C_i(q_i(t),\dot{q}_i(t))\dot{q}_i(t) + g_i(q_i(t)) = \tau_i(t), \quad i \in \mathcal{V}. \tag{3}$$

The aforementioned properties are adoptable for these equations in the same way.

2.3 Problems formulation

The formation discussed in this article will focus on the relative displacement of paired robots. Let $\mathcal{H} \in \mathbb{R}^{p\times n}$ be the frame of expected formation, which is expressed by a stack vector $\mathcal{H} = [h_1, h_2, \ldots, h_n]^{\mathrm{T}}$, where $h_i \in \mathbb{R}^p$, $i \in \mathcal{V}$. In that, $(h_i - h_j)$, $i, j \in \mathcal{V}$ presented expected formation. Let $s_i(t) = \int_0^t q_i(u) - h_i \,\mathrm{d}u$ be the relative error of formation for robot $i \in \mathcal{V}$. It induces that the local formation observer of robot-i is $r_i(t) \doteq \dot{s}_i(t) = q_i(t) - h_i$.

Considering that $\mathcal{H}$ is constant formation, the tracking objective is defined as a real function $\mathcal{J}(t) \in \mathbb{R}^p$. Let $B = \mathrm{diag}(b_1, b_2, \ldots, b_n)$ be the matrix for tender, in which b_i $(i \in \mathcal{V})$ are non-negative elements in $\mathbb{R}$. For robot-i, the tracking error is estimated by $\bar{q}_i(t) = q_i(t) - b_i\mathcal{J}(t)$. As $\bar{s}_i = \int_0^t r_i(u) - b_i\mathcal{J}(u)\mathrm{d}u$ is local error of formation tracking, the formation tracking will be observed by $\bar{r}_i \doteq \dot{\bar{s}}_i = r_i(t) - b_i\mathcal{J}(t)$. It should note $\bar{r}_i = \bar{q}_i(t) - h_i$.

It is left to infer the basics of finite-time control for main work. Give that $x = [x_1(t), x_2(t), \ldots, x_m(t)]^{\mathrm{T}}$ is arbitrary real vector (stack). The function $\mathrm{sig}^{\alpha}(x(t)) \doteq f_{\alpha}(x(t))$ at $\alpha > 0$ is defined as

$$\mathrm{sig}^{\alpha}(x(t)) = [\mathrm{sig}^{\alpha}(x_1(t)), \mathrm{sig}^{\alpha}(x_2(t)), \ldots, \mathrm{sig}^{\alpha}(x_m(t))]^{\mathrm{T}}, \tag{4}$$

where $\mathrm{sig}^{\alpha}(x_i(t)) = \mathrm{sign}(x_i(t))|x_i(t)|^{\alpha}$. Observe that $\mathrm{sig}^{\alpha}(x(t))$ is continuously differentiable except for the m orthogonal hyper-planes passing through the origin. Thus, the derivation of $f_{\alpha}(x(t))$ can be defined as $\alpha\mathrm{sign}(x(t))\mathrm{sig}^{\alpha-1}(x(t))$. Moreover, $x(t)^{\mathrm{T}}\mathrm{sig}^{\alpha}(x(t)) \geqslant 0$. Let $\|\cdot\|_b$ be b-norm and $\|x(t)\|$ be the 2-norm of $x(t)$.

Lemma 4 ([28]). For $\alpha \in (0, 1)$, the following inequalities hold:

$$(\|x(t)\|_1)^{\alpha} \leqslant \|x(t)\|_{\alpha}, \tag{5}$$

$$\|x(t)\|^{\alpha} \leqslant (\|x(t)\|_{\alpha})^2. \tag{6}$$

Lemma 5 ([28]). $V(x(t))$ is positive definite function defined in $x(t) \in \mathbb{R}^m$. If there exist $0 < a < 1$ and $0 < \beta$ such that $\dot{V}(x(t)) + \beta V^a(x(t)) \leqslant 0$ for $x(t) \in U_{\mathbf{0}}/\{\mathbf{0}\}$, then $V(x(t))$ will converge to the origin in finite time T, and the settling time depend on $x(0)$, $T \leqslant \frac{V^{1-\alpha}(0)}{\beta(1-\alpha)}$.

If Lemma 5 holds for nonlinear system $\dot{x}(t) = g(x(t))$ with initial conditions $x(0)$ and $g(0) = 0$, the system will be said to be local finite-time stable.

Lemma 6 ([28]). If $y^{(k)}(t)$ is continuous and bounded on $[0, t^*]$ and $\lim_{t\to t^*} y(t)$ exists, then $y(t)^{(\ell)}$ converges to the origin in finite time t^* for any $1 \leqslant \ell \leqslant k$.

Definition 1. (1) If there exists positive $t^* \in \mathbb{R}$ such that $\phi_i r_i(t) - \phi_j r_j(t) = 0$ and $\dot{q}_i = 0$ for $i, j \in \mathcal{V}$ as $t > t^*$, then MRSs reach formation consensus of $\mathcal{H}$ in finite time t^*. (2) If $r_i(t) = b_i\mathcal{J}(t)$ for $t > t^*$, $i \in \mathcal{V}$, then MRSs achieve formation tracking of $(\mathcal{H}, \mathcal{J}(t))$ in finite time t^*.

Observe that the tracking information will be distributed by tender elements b_i. For $b_i \neq 0$, robot-i will refer to the tracking information. Otherwise, robot-i will not make tracking.

Remark 1. If formation tracking, $r_i(t) = b_i\mathcal{J}(t)$ results in $\dot{q}_i(t) = b_i\dot{\mathcal{J}}(t)$ as well as $\phi_i r_i(t) - \phi_j r_j(t) = (\phi_i b_i - \phi_j b_j)\mathcal{J}(t)$. The equation $\dot{q}_i(t) = b_i\dot{\mathcal{J}}(t)$ essentially presents the formation tracking. From $\phi_i r_i(t) - \phi_j r_j(t) = (\phi_i b_i - \phi_j b_j)\mathcal{J}(t)$, the formation will be determined by signed element ϕ_i and tracking tender b_i. Moreover, Figure 2 gives explicit demonstration as b_i are chosen as 0-1 variables. It is applicable in practical scenes, such as patrolling and guarding multiple positions, guidance, and protection for navigation, and point-line parallel processing in manufacturing.

3 Main results

This section provides solutions to finite-time consensus problems of formation control. It contributes to providing adaptive finite-time formation protocols. The conditions sufficient for finite-time formation consensus are verified, which contributes to providing adaptive finite-time formation protocols. Then, the adaptive finite-time formation protocols will be discussed for formation tracking.

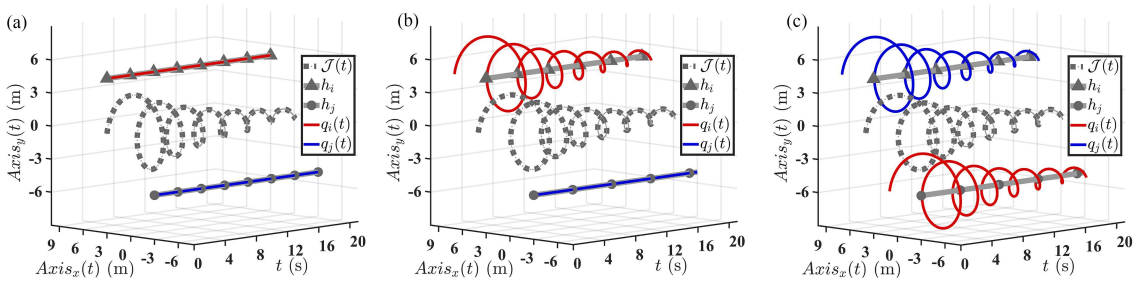

Figure 2 (Color online) Demonstration of formation tracking. (a) $b_i = 0, b_j = 0$; (b) $b_i = 1, b_j = 0$; (c) $b_i = 1, b_j = 1$.

3.1 Formation consensus in finite-time

Regarding the complex behavior with formation $\mathcal{H}$, it is the basement to make MRSs be aligned in formation. The next is going to provide the finite-time protocols for MLSs' formation consensus.

Defining the reference vector for robot $i \in \mathcal{V}$,

$$q_{ri}(t) = -\sum_{j\in\mathcal{V}} a_{ij}\left(\phi_i r_i(t)\phi_j - r_j(t)\right) - \beta f_\alpha(\epsilon_i(t)), \tag{7}$$

where $0 < \alpha < 1$, $\beta \geqslant 0$, and ϵ_i is sliding vector defined as

$$\epsilon_i(t) = q_i(t) + \sum_{j\in\mathcal{V}} a_{ij}\left(\phi_i s_i(t)\phi_j - s_j(t)\right). \tag{8}$$

It gives

$$\dot{\epsilon}_i(t) = \dot{r}_i(t) + \sum_{j\in\mathcal{V}} a_{ij}\left(\phi_i r_i(t)\phi_j - r_j(t)\right). \tag{9}$$

Then, the error vector is defined by

$$\xi_i(t) = \dot{q}_i(t) - q_{ri}(t), \tag{10}$$

which leads to

$$\dot{\epsilon}_i(t) = \xi_i(t) - \beta f_\alpha(\epsilon_i(t)). \tag{11}$$

Under these denotations, the control protocols are given as

$$\tau_i(t) = Y_i\left(q_i(t), \dot{q}_i(t), \dot{q}_{ri}(t), q_{ri}(t)\right)\hat{\theta}_i(t) - K_1\xi_i(t) - K_2 f_\alpha(\xi_i(t)),\ i \in \mathcal{V}, \tag{12}$$

where $K_1 > 0$ and $K_2 > 0$ are diagonal matrices, and $\hat{\theta}_i(t)$ is the estimate of θ_i. And the estimate error $\tilde{\theta}_i(t) = \hat{\theta}_i(t) - \theta_i$ obeys the law

$$\dot{\tilde{\theta}}_i(t) = -\Gamma_i Y_i^{\mathrm{T}}\left(q_i(t), \dot{q}_i(t), \dot{q}_{ri}(t), q_{ri}(t)\right)\xi_i(t),\ i \in \mathcal{V}, \tag{13}$$

where Γ_i is symmetric positive definite matrix. After substituting (12) and (13) into systems (3), there are closed-loop systems

$$M_i(q_i(t))\dot{\xi}_i(t) + C_i(q_i(t), \dot{q}_i(t))\xi_i(t) + K_1\xi_i(t) + K_2 f_\alpha(\xi_i(t)) = Y_i\left(q_i(t), \dot{q}_i(t), \dot{q}_{ri}(t), q_{ri}(t)\right)\tilde{\theta}_i(t), i \in \mathcal{V}. \tag{14}$$

Before giving the main results, it is needed to resort the above symbols into compact forms. First, let $q(t)$, $q_r(t)$, $\xi(t)$, and $\epsilon(t)$ be the stack vector of column vector sequences $\{q_i(t)|i \in \mathcal{V}\}$, $\{q_{ri}(t)|i \in \mathcal{V}\}$, $\{\xi_i(t)|i \in \mathcal{V}\}$, and $\{\epsilon_i|i \in \mathcal{V}\}$, respectively. Let $M(q(t))$, $C(q(t), \dot{q}(t))$, and $Y(q(t), \dot{q}(t), \ddot{q}_r(t), \dot{q}_r(t))$ be the block diagonal matrix of $\{M_i(q_i(t))|i \in \mathcal{V}\}$, $\{C_i(q_i(t), \dot{q}_i(t))|i \in \mathcal{V}\}$, and $\{Y_i(q_i(t), \dot{q}_i(t), \ddot{q}_{ri}(t), \dot{q}_{ri}(t))|i \in \mathcal{V}\}$, respectively. $g(q(t))$ naturally is the column stack vector arranged in order of $\{g_i(q_i(t))|i \in \mathcal{V}\}$. θ is also such a column stack vector of $\{\theta_i|i \in \mathcal{V}\}$. Moreover, the analysis of p-dimensional vectors is discussed below using the Kronecker product

$$M \otimes N = \begin{bmatrix} m_{11}N & m_{12}N & \dots & m_{1m}N \\ m_{21}N & m_{22}N & \dots & m_{2m}N \\ \vdots & \vdots & \vdots & \vdots \\ m_{m1}N & m_{m2}N & \dots & m_{mm}N \end{bmatrix}_{mn\times mn},$$

where $M = [m_{ij}]_{m\times m}$, $N = [n_{ij}]_{n\times n}$. Then, Eqs. (9) and (11) can be rewritten as

$$\dot{q}(t) = \dot{\epsilon}(t) - (L \otimes I_p)r(t), \tag{15}$$

$$\dot{\epsilon}(t) = \xi(t) - \beta f_\alpha(\epsilon_i(t)). \tag{16}$$

The closed-loop systems (14) can be formed by

$$M(q(t))\dot{\xi}(t) + C(q(t), \dot{q}(t))\xi(t) + \Delta_1\xi(t) + \Delta_2 f_\alpha(\xi(t)) = Y\left(q(t), \dot{q}(t), \dot{q}_r(t), q_r(t)\right)\tilde{\theta}, \tag{17}$$

where $\Delta_1 = (K_1 \otimes I_p)$, $\Delta_2 = (K_2 \otimes I_p)$.

Under the work, the finite-time formation consensus is given below.

Theorem 1. With the control protocols (12) and estimate laws (13), the MLSs (3) will reach formation consensus of $\mathcal{H}$ in finite time.

Proof. The proof is equivalent to discuss the systems (16) and (17), which will be finished by two steps. The first is to clarify that all defined variables are bounded. The second is to analyze the finite-time stability of formation consensus for systems (17).

(1) Bounded variables. For systems (17), the Lyapunov candidate is selected as

$$V_b(t) = \frac{1}{2}\sum_{i\in\mathcal{V}}\left(\xi_i^{\mathrm{T}}(t)M_i(q_i(t))\xi_i(t) + \tilde{\theta}_i^{\mathrm{T}}(t){\Gamma_i}^{-1}\tilde{\theta}_i(t)\right). \tag{18}$$

According to Lemma 2, it is derived from the following equation:

$$\dot{V}_b(t) = -\sum_{i\in\mathcal{V}}\left(\xi_i^{\mathrm{T}}(t)K_2 f_\alpha(\xi_i(t)) + \xi_i^{\mathrm{T}}(t)K_1\xi_i(t)\right). \tag{19}$$

As is discussed in Subsection 2.3, $\xi_i^{\mathrm{T}}(t)K_2 f_\alpha(\xi_i(t)) \geqslant 0$ holds. Thus, it has $\dot{V}_b(t) \leqslant 0$. As results, $\xi_i(t)$ and $\tilde{\theta}_i(t)$ are bounded. Observe that Eq. (16) presents the input-to-state stable system regarding the input $\xi(t)$ and state $\epsilon(t)$. Thus, $\epsilon_i(t)$, $\dot{\epsilon}_i(t)$ are bounded.

(2) Finite-time convergence. Choose the second Lyapunov candidate as

$$V^*(t) = \frac{1}{2}\sum_{i\in\mathcal{V}}\xi_i^{\mathrm{T}}(t)M_i(q_i(t))\xi_i(t). \tag{20}$$

It has that

$$\dot{V}^*(t) = -\sum_{i\in\mathcal{V}}\left(\xi_i^{\mathrm{T}}(t)K_2 f_\alpha(\xi_i(t)) + \xi_i^{\mathrm{T}}(t)K_1\xi_i(t) - \xi_i^{\mathrm{T}}(t)Y_i(t)\tilde{\theta}_i(t)\right), \tag{21}$$

in which $Y_i(t) = Y_i\left(q(t), \dot{q}(t), \dot{q}_r(t), q_r(t)\right)$. From Cauchy-Schwarz Inequality, it has that $\xi_i^{\mathrm{T}}(t)Y_i(t)\tilde{\theta}_i(t) \leqslant \|\xi_i(t)\|\|Y_i(t)\tilde{\theta}_i(t)\|$. Then, one can select diagonal matrix K_1 to obtain inequality $\sum_{i\in\mathcal{V}}(\xi_i^{\mathrm{T}}K_1\xi_i - \xi_i^{\mathrm{T}}Y_i\tilde{\theta}_i) > 0$ since boundedness properties hold (Lemma 1). It thus deduces that

$$\dot{V}^*(t) \leqslant -\sum_{i\in\mathcal{V}}\xi_i^{\mathrm{T}}(t)K_2 f_\alpha(\xi_i(t)). \tag{22}$$

Let κ be the minimum diagonal entries of K_1, from Lemma 4,

$$\dot{V}^*(t) \leqslant -\kappa\sum_{i\in\mathcal{V}}\left(\|\xi_i(t)\|^2\right)^{\frac{1+\alpha}{2}}. \tag{23}$$

As is given in Lemma 1, $M_i(q_i(t))$ has infimum b_{M_i}. It provides that

$$V^*(t) \leqslant \frac{1}{2}\sum_{i\in\mathcal{V}} b_{M_i}\|\xi_i(t)\|^2. \tag{24}$$

Combining (23) with (24), one has

$$\dot{V}^*(t) \leqslant -\varrho^\gamma\kappa(V^*(t))^\gamma, \tag{25}$$

where $\gamma = \frac{1+\alpha}{2}$, $\rho = \max_{i\in\mathcal{V}}\{b_{M_i}\}$, $\varrho = \frac{2}{\rho}$. From Lemma 5, $V^*(t)$ converges to the origin in finite time, and the setting time satisfies $t^* \leqslant \frac{1}{\rho^\gamma \kappa(1-\gamma)}(V^*(0))^{1-\gamma}$. With the boundedness property of variables, $\xi_i(t)$ will converge to the origin in the setting finite-time t^*. Since Eq. (16) presents the input-to-state stable system, both $\epsilon_i(t)$ and $\dot{\epsilon}_i(t)$ converge to the origin in finite time. By applying $\Psi_i\Phi$ on the both side of (15), it obtains that

$$(\bar{q}_i(t)\Phi \otimes I_p)\,\dot{q}(t) = (\Psi_i\Phi \otimes I_p)\,\dot{\epsilon}(t) - (\Psi_i\Phi L\Phi\Psi_i^{-1} \otimes I_p)\,(\Psi_i\Phi \otimes I_p)\,r(t). \tag{26}$$

From the previous discussion of matrices (1), one has

$$(\pi^{\mathrm{T}}\Phi \otimes I_3)\dot{q}(t) = (\pi^{\mathrm{T}}\Phi \otimes I_3)\dot{\epsilon}(t) \tag{27}$$

and

$$\begin{bmatrix} \phi_1\dot{q}_1(t) - \phi_i\dot{q}_i(t) \\ \vdots \\ \phi_{i-1}\dot{q}_{i-1}(t) - \phi_i\dot{q}_i(t) \\ \phi_{i+1}\dot{q}_{i+1}(t) - \phi_i\dot{q}_i(t) \\ \vdots \\ \phi_n\dot{q}_n(t) - \phi_i\dot{q}_i(t) \end{bmatrix} = \begin{bmatrix} \phi_1\dot{\epsilon}_1(t) - \phi_i\dot{\epsilon}_i(t) \\ \vdots \\ \phi_{i-1}\dot{\epsilon}_{i-1}(t) - \phi_i\dot{\epsilon}_i(t) \\ \phi_{i+1}\dot{\epsilon}_{i+1}(t) - \phi_i\dot{\epsilon}_i(t) \\ \vdots \\ \phi_n\dot{\epsilon}_n(t) - \phi_i\dot{\epsilon}_i(t) \end{bmatrix} - (L_i \otimes I_p) \begin{bmatrix} \phi_1 r_1(t) - \phi_i r_i(t) \\ \vdots \\ \phi_{i-1} r_{i-1}(t) - \phi_i r_i(t) \\ \phi_{i+1} r_{i+1}(t) - \phi_i r_i(t) \\ \vdots \\ \phi_n r_n(t) - \phi_i r_i(t) \end{bmatrix}. \tag{28}$$

Note that Eq. (28) is input-to-state stable since L_i is Hurwitz matrix. Consider that $\dot{\epsilon}_i\Psi_i$ converges to origin in finite time, and

$$\begin{bmatrix} \phi_1\dot{q}_1 - \phi_i\dot{q}_i \\ \vdots \\ \phi_{i-1}\dot{q}_{i-1} - \phi_i\dot{q}_i \\ \phi_{i+1}\dot{q}_{i+1} - \phi_i\dot{q}_i \\ \vdots \\ \phi_n\dot{q}_n - \phi_i\dot{q}_i \end{bmatrix} \text{ and } \begin{bmatrix} \phi_1 r_1 - \phi_i r_i \\ \vdots \\ \phi_{i-1} r_{i-1} - \phi_i r_i \\ \phi_{i+1} r_{i+1} - \phi_i r_i \\ \vdots \\ \phi_n r_n - \phi_i r_i \end{bmatrix}$$

converge to origin in finite time t^*. Combining this result with (27), $(\Psi_i\Phi \otimes I_p)\,\dot{q}(t) = \mathbf{0}$ for $t > t^*$. This gives that $\dot{q}(t) = \mathbf{0}$ as $t > t^*$ since $\Psi_i\Phi$ is inevitable. Moreover, for all $i, j \in \mathcal{V}$, $\phi_i r_i(t) - \phi_j r_j(t) = \mathbf{0}$ at $t > t^*$. This implies that the discussed MLSs are said to reach the consensus of formation $\mathcal{H}$ in finite time. Consequently, the proof is finished.

Remark 2. Different with [21,23], this research work introduces two sliding vectors $\xi_i(t)$ and $\epsilon_i(t)$, and then inserts finite-time items $f_\alpha(\xi_i(t))$ and $f_\alpha(\epsilon_i(t))$ into torque protocols. It should be noted that the protocols (12) will be a general way to realize formation control if $K_2 = 0$. Refs. [24,25] have introduced variables to realize finite-time control for Lagrange robots. However, those control protocols neglect the uncertain parameters of Lagrange robots. Two kinds of sliding mode variables ξ_i and ϵ_i essentially define virtual controllers for each system. The virtual controllers are meant for finite-time control of the intermediate variables of each system. In the proof, the system error variable of the closed-loop system ξ converges to the origin in finite time by deduction using Lyapunov analysis. However, Lagrange systems are nonlinear systems with uncertain parameters, which will lead to the fact that neither the state q of the system nor its derivative $\dot{q}$ can be analyzed by using the chain rules as in the case of general linear systems. Nevertheless, the virtual controller ϵ is given in this paper, which provides a way to analyze the state of MLSs. In conclusion, it can be seen that the combined use of ξ and ϵ is the key to accomplishing the system analysis. Therefore, these two are referred to as coupled sliding mode variables in the paper.

Remark 3. Regarding a non-signed graph $\mathcal{G}$, $\phi_i q_i(t) - \phi_j q_j(t)$ presents the relative coordinates of robots i and j. If $\mathcal{G}$ is a signed graph, $\phi_i q_i(t) - \phi_j q_j(t)$ should be discussed into two cases. Consider the case of $\phi_i\phi_j = -1$, $\phi_i q_i(t) - \phi_j q_j(t)$ will present the center of robot-i and robot-j. Therefore, $\phi_i r_i(t) - \phi_j r_j(t) = 0$ implies that robot-i and robot-j will reach a center consensus of $h_i + h_j$. In addition, $\dot{q}_i(t)$ and $\dot{q}_j(t)$ reach to $\mathbf{0}$ in the process of $\phi_i\dot{q}_i(t) - \phi_j\dot{q}_j(t) = 0$. At this point, robots i and j will be aligned bidirectionally through $h_i + h_j$ in the case of $\phi_i\phi_j = -1$.

The aforementioned formation consensus will be further expanded after the next verification of tender tracking.

3.2 Formation tracking in finite time

For reaching the expected placement, it is necessary to exploit the MLSs' tracking performance. Thus, the following work focuses on finite-time control of formation tracking.

The reference velocity of robot-i is defined as

$$\bar{q}_{ri}(t) = b_i\dot{\mathcal{J}}(t) - \sum_{j\in\mathcal{V}} a_{ij}\left(\phi_i\bar{r}_i(t)\phi_j - \bar{r}_j(t)\right) - \beta f_\alpha(\varepsilon_i(t)), \tag{29}$$

where

$$\varepsilon_i = \bar{q}_i(t) + \sum_{j\in\mathcal{V}} a_{ij}\left(\phi_i\bar{s}(t)_i\phi_j - \bar{s}_j(t)\right). \tag{30}$$

Then, one has

$$\dot{\varepsilon}_i(t) = \dot{\bar{r}}(t) + \sum_{j\in\mathcal{V}} a_{ij}\left(\phi_i\bar{r}_i(t)\phi_j - \bar{r}(t)_j\right). \tag{31}$$

The global velocity error of robot-i is given by

$$\bar{\xi}_i(t) = \dot{q}_i(t) - \bar{q}_{ri}(t) = \dot{\varepsilon}_i(t) + \beta f_\alpha(\varepsilon_i(t)). \tag{32}$$

The control protocols will be given in the same way. Let the control protocols be

$$\tau_i(t) = Y_i\left(q_i(t), \dot{q}_i(t), \dot{\bar{q}}_{ri}(t), \bar{q}_{ri}(t)\right)\hat{\theta}_i(t) - K_1\bar{\xi}_i(t) - K_2 f_\alpha(\bar{\xi}_i(t)),\ i\in\mathcal{V}, \tag{33}$$

and let the estimate errors obey

$$\dot{\tilde{\theta}}_i(t) = -\Gamma_i Y_i^{\mathrm{T}}\left(q_i(t), \dot{q}_i(t), \dot{\bar{q}}_{ri}(t), \bar{q}_{ri}(t)\right)\bar{\xi}_i(t),\ i\in\mathcal{V}. \tag{34}$$

The tender-tracking problems discussed in this paper need to meet the following assumptions.

Assumption 3. $B\mathcal{J}(t)$ is bounded. That is, there exists a positive constant $b_{\mathcal{J}}$ such that $\|B\mathcal{J}(t)\| \leqslant b_{\mathcal{J}}$.

For the finite time formation problems, the article gives the solution at Theorem 1. However, for the tracking problems, the objective is time-varying. The following Theorem 2 further adds the tracking objective for the closed-loop system of Theorem 1, which is equivalent to adding an external disturbance. In general, bounded external perturbations are an essential requirement for adaptive control. Thus, Assumption 3 requires the tracking signal to be bounded.

Theorem 2. With the control protocols (33) and estimate laws (13), the MLSs (3) will achieve formation tracking of $(\mathcal{H}, \mathcal{J}(t))$ in finite time.

Proof. Similar with Theorem 1, it also obtains a differential equation about variables $\bar{\xi}(t)$,

$$M(q)\dot{\bar{\xi}}(t) + C(q,\dot{q}(t))\bar{\xi}(t) + \Delta_1\bar{\xi}(t) + \Delta_2 f_\alpha(\bar{\xi}(t)) = Y\left(q(t),\dot{q}(t),\dot{\bar{q}}_r(t),\bar{q}_r(t)\right)\tilde{\theta}(t). \tag{35}$$

In the same way, select the following Lyapunov candidates:

$$\bar{V}_b(t) = \frac{1}{2}\left(\bar{\xi}(t)M(q(t))\bar{\xi}(t) + \tilde{\theta}^{\mathrm{T}}(t)\Gamma^{-1}\tilde{\theta}(t)\right), \tag{36}$$

$$\bar{V}^*(t) = \frac{1}{2}\bar{\xi(t)}M(q(t))\bar{\xi(t)}, \tag{37}$$

where Γ is the block diagonal matrix of $\{\Gamma_i | i\in\mathcal{V}\}$. By analyzing Lyapunov candidate (36), $\bar{\xi}(t)$, $\tilde{\theta}(t)$, $\varepsilon(t)$, and $\dot{\varepsilon}(t)$ are bounded. Moreover, from (30), it has

$$\varepsilon(t) - (\mathbf{1}_n\otimes\mathcal{H}) = \dot{\bar{s}}(t) + (L\otimes I_p)\,\bar{s}(t). \tag{38}$$

Eq. (38) is input-to-state stable with respect to the input $\varepsilon(t) - (\mathbf{1}_n\otimes\mathcal{H})$ and state $\bar{s}(t)$. Combining Eq. (38) with Assumption 3, $\bar{s}$ and $\dot{\bar{s}}$ are bounded.

Table 1 Physical parameters of 8 robots[a)]

	Robot1	Robot2	Robot3	Robot4	Robot5	Robot6	Robot7	Robot8
m_{i1}	1.4	1.6	1.8	2	2.2	2.4	2.6	2.8
m_{i2}	1.52	1.64	1.76	1.88	2	2.12	2.24	2.36
ℓ_{i1}	1.88	1.96	2.04	2.12	2.2	2.28	2.36	2.44
ℓ_{i2}	2.34	2.38	2.42	2.46	2.5	2.54	2.58	2.62

a) Control parameters for all simulation are selected as $\alpha = 0.333$, $\beta = \mathbf{1}_8 \otimes \mathcal{X}$, $K_1 = \mathbf{1}_8 \otimes \mathcal{Y}$, $K_2 = 10\mathcal{Z} \otimes I_2$, and $\Gamma = 3 \otimes I_{16}$, where $\mathcal{X} = \mathrm{diag}(0.1885, 0.1881)$, $\mathcal{Y} = \mathrm{diag}(39, 48)$, and $\mathcal{Z} = \mathrm{diag}(2, 6, 3, 2, 3, 2, 2, 2)$.

With Lyapunov candidate (37), it has that $\bar{\xi}(t)$ will converge to the origin in finite-time, in which $\bar{t} \leqslant \frac{1}{\rho^{\gamma}\kappa(1-\gamma)}(\bar{V}^*(0))^{1-\gamma}$ satisfies. As results, $\varepsilon(t)$ and $\dot{\varepsilon}(t)$ converge to origin in finite time. Observe that Eq. (31) can be rewritten in compact form:

$$\dot{\bar{r}}(t) = \dot{\varepsilon}(t) - (L \otimes I_p)\bar{r}(t). \tag{39}$$

This leads to $\dot{\bar{q}}(t) \to \mathbf{0}$ in finite-time $\bar{t}$, which implies $\dot{q}_i(t) = b_i\dot{\mathcal{J}}(t)$ for all $t \geqslant \bar{t}$. Thus, $\bar{r}(t)$ and $\dot{\bar{r}}(t)$ are bounded. Note that Eq. (39) also gives that $\phi_i\bar{r}_i(t) - \phi_j\bar{r}_j(t)$ converge to $\mathbf{0}$ in finite time. Therefore, $\phi_i r_i(t) - \phi_j r_j(t) = (\phi_i b_i - \phi_j b_j)\mathcal{J}(t)$ as $t \geqslant \bar{t}$. As is given before, $\bar{s}(t)$, $\bar{r}(t)$, $\dot{\bar{r}}(t)$, and $B\mathcal{J}(t)$ are bounded. From Lemma 6, $\bar{r}(t)$ will converge to $\mathbf{0}$ in finite time. Thus, $r(t) = (B \otimes I_p)(\mathbf{1}_n \otimes \mathcal{H})$ for $t \geqslant \bar{t}$. With the above conclusion, the MLSs (3) reach formation tracking of $(\mathcal{H}, \mathcal{J}(t))$ in finite time.

As for $\phi_i\phi_j = -1$, Remark 3 concludes that robot-i and robot-j display bidirectional coordination of center-aligned consensus. From the proof of finite-time tracking, the formation tracking performance depends on selecting network topology and tender values.

Remark 4. Select 0-1 variables as tender elements, robot-i and robot-j will reach a formation tracking consensus of $\phi_i(h_i + b_i\mathcal{J}(t)) - \phi_j(h_j + b_j\mathcal{J}(t))$. Different from the formation consensus, the center-aligned consensus will not appear in the formation track. Whether for $\phi_i\phi_j = 1$ or for $\phi_i\phi_j = -1$, robot-i and robot-j will track $\mathcal{J}(t)$ with the formation consensus of $h_i - h_j$. Nevertheless, it should be noted that the direction of tracking will be symmetric for $\phi_i\phi_j = -1$.

4 Simulations

This section is arranged with three sets of comparative experiments, which are the comparative simulation of MLSs' formations under finite-time control protocols and non-finite-time control protocols, the comparative simulation of MLSs' finite-time formations under non-bilateral network topology and bilateral network topology, and the comparative simulation of MLSs' finite-time formations tracking pairs based on different tenders' signals. Further, we add a discussion on the results of these three sets of comparison experiments.

Due to the length of the paper, we have chosen to conduct our experiments with a kinetic model that satisfies Assumptions 1–3. All the following experiments uniformly select 8 Lagrange robots having the kinetic coefficients expressed by

$$M_i(q_i) = \begin{bmatrix} u_{i1} + 2u_{i2}c(q_{i2}) & u_{i3} + u_{i2}c(q_{i2}) \\ u_{i3} + u_{i2}c(q_{i2}) & u_{i3} \end{bmatrix}, \; C_i(q_i, \dot{q}_i) = \begin{bmatrix} u_{i2}\dot{q}_{i2}s(q_{i2}) & -u_{i2}(\dot{q}_{i1} + \dot{q}_{i2})s(q_{i2}) \\ u_{i2}\dot{q}_{i1}s(q_{i2}) & 0 \end{bmatrix},$$

$$g(q_i) = \begin{bmatrix} 9.8u_{i4}\dot{q}_{i2}c(q_{i1}) + 9.8u_{i5}c(q_{i1} + q_{i2}) \\ 9.8u_{i5}c(q_{i1} + q_{i2}) \end{bmatrix},$$

where the physical parameters are given in Table 1 and Figure 3. The data in Table 1 are the parameters of the parameter-identified Lagrange kinetic model.

From Lemma 3, the kinetic constant vector is selected as $\theta_{i1} = m_{i1}\ell_{i1}^2 + m_{i2}(\ell_{i1}^2 + \ell_{i2}^2) + J_{i1} + J_{i2}$, $\theta_{i2} = \frac{1}{2}m_{i2}\ell_{i1}^2$, $\theta_{i3} = \frac{1}{4}m_{i2}\ell_{i2}^2 + J_{i2}$, $\theta_{i4} = \frac{1}{2}m_{i1}\ell_{i1} + m_{i2}\ell_{i1}$, $\theta_{i5} = \frac{1}{2}m_{i2}\ell_{i2}$, where m_{ip} (kg) is the link mass, ℓ_{ip} (m) is the link length, and $J_{ip} = \frac{1}{12}m_{ip}\ell_{ip}^2(kg \cdot m^2)$, $p = 1, 2$. Then the explicit expression of the regression matrix is

$$Y_i = \begin{bmatrix} \dot{x} & Y_{i21} & \dot{x} & 9.8\dot{q}_{i2}\cos(q_{i1}) & 9.8\cos(q_{i1} + q_{i2}) \\ 0 & Y_{i22} & \dot{x} + \dot{y} & 0 & 9.8\cos(q_{i1} + q_{i2}) \end{bmatrix},$$

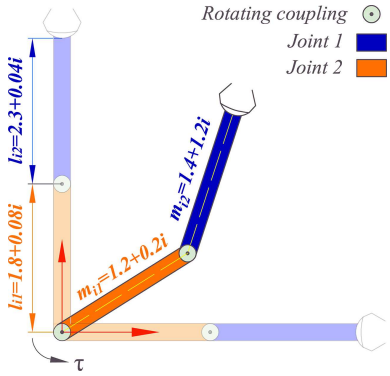

Figure 3 (Color online) Two-link manipulators.

where $Y_{i21} = 2\cos(q_{i2})\dot{x} + \cos(q_{i2})\dot{y} + \dot{q}_{i2}\sin(q_{i2})x - (\dot{q}_{i1} + \dot{q}_{i2})\sin(q_{i2})y$, $Y_{i22} = \cos(q_{i2})\dot{x} + \dot{q}_{i1}\sin(q_{i2})x$.

Further, the information interaction networks of the above 8 robots include a non-bipartite topology represented by Figure 1(a), and a bipartite topology corresponding to Figure 1(b). For the formation problems, the networked MLSs will reach formation consensus on $\mathcal{H}_1$ (positive octagon), $\mathcal{H}_2$ (number 4), $\mathcal{H}_3$ (double square), and $\mathcal{H}_4$ (positive triangle and positive pentagon), referring to equations of (40)–(43).

$$\mathcal{H}_1 = \begin{bmatrix} 0.51 & 2.04 & 4.59 & 6.12 & 6.12 & 4.59 & 2.04 & 0.51 \\ 2.55 & 0.51 & 0.51 & 2.55 & 5.10 & 7.14 & 7.14 & 5.10 \end{bmatrix}, \tag{40}$$

$$\mathcal{H}_2 = \begin{bmatrix} 7.00 & 5.00 & 3.00 & 9.00 & 8.50 & 6.50 & 4.50 & 8.50 \\ 3.00 & 5.00 & 7.00 & 1.00 & 7.50 & 5.50 & 3.50 & 1.50 \end{bmatrix}, \tag{41}$$

$$\mathcal{H}_{3i} = \begin{cases} 1.25 \times \begin{bmatrix} \cos(\frac{\pi i}{2} - \frac{\pi}{2}) + 1 \\ \sin(\frac{\pi i}{2} - \frac{\pi}{2}) + 1 \end{bmatrix}, & i = 1, 2, 3, 4, \\ 3.30 \times \begin{bmatrix} \cos(\frac{\pi i}{2} - \frac{3\pi}{2}) + 1 \\ \sin(\frac{\pi i}{2} - \frac{3\pi}{2}) + 1 \end{bmatrix}, & i = 5, 6, 7, 8, \end{cases} \tag{42}$$

$$\mathcal{H}_{4i} = \begin{cases} 2.30 \times \begin{bmatrix} \cos(\frac{2\pi i}{3}) - 1 \\ \sin(\frac{2\pi i}{3}) - 1 \end{bmatrix}, & i = 1, 2, 3, \\ 4.60 \times \begin{bmatrix} \cos(\frac{2\pi i}{5}) - 1 \\ \sin(\frac{2\pi i}{5}) - 1 \end{bmatrix}, & i = 4, 5, 6, 7, 8. \end{cases} \tag{43}$$

In particular, binary numbers are chosen as tender elements. The networked MLSs will track $\mathcal{J}(t)$ according to the tenders B_1 and B_2.

$$\mathcal{J}(t) = \begin{bmatrix} 3\mathrm{e}^{\frac{-t}{10}}\sin(2t) \\ 3\mathrm{e}^{\frac{-t}{10}}\cos(2t) \end{bmatrix}. \tag{44}$$

Unless otherwise stated, the control parameters of all the following simulation systems are uniformly given in Table 1.

4.1 Formation performances of finite-time control

The first part will carry out the formation consensus of MLSs under complex topology $\mathcal{G}_1$, which is given by controlled simulations for finite-time control and infinite-time control. Using $\mathcal{G}_1$ (Figure 1(a)) as the network topology of the controlled MLSs, three sets of pairwise simulations are performed in the first part of the experiment for the formations with and without the finite-time protocols. The desired formations are $\mathcal{H}_1$, $\mathcal{H}_2$, and $\mathcal{H}_3$.

Under the finite-time control protocol, the formation performances of MLSs behave as in Figure 4. In addition, MLSs formations without adding finite-time control are also considered in this part of the experiment. The comparison results are given below. Figures 5(a)–(c) correspond to the convergence

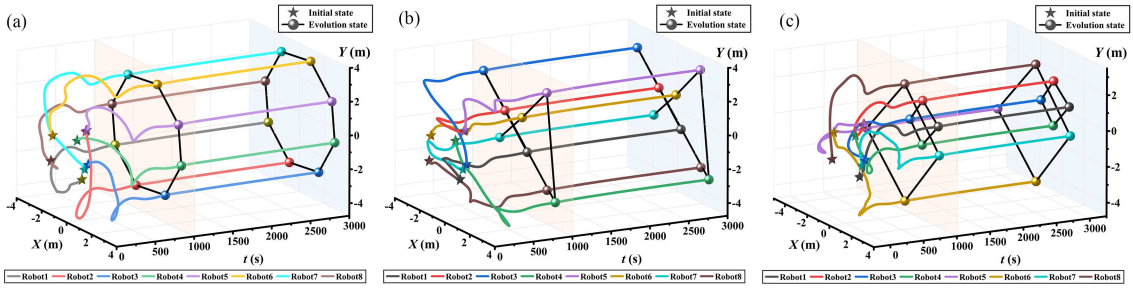

Figure 4 (Color online) Finite-time formation under $\mathcal{G}_1$. (a) $\mathcal{H}_1$: positive octagon; (b) $\mathcal{H}_2$: number 4; (c) $\mathcal{H}_3$: double square.

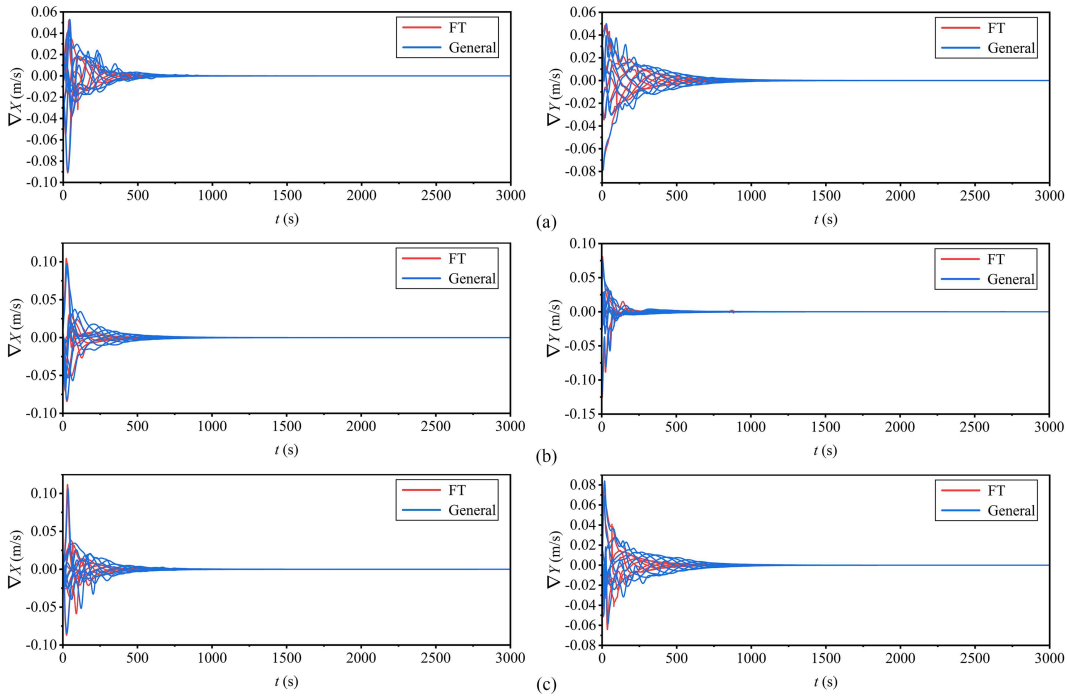

Figure 5 (Color online) Comparisons of convergence gradients. (a) Formation of $\mathcal{H}_1$; (b) formation of $\mathcal{H}_2$; (c) formation of $\mathcal{H}_3$.

gradients of the above three sets of compared controlled systems, respectively. From these three sets of comparisons, it can be concluded that the gradients of the finite-time control system are always internally contained in the gradients of systems without finite-time control.

Remark 5. Considering the above implementation of the simulated control system is solved using the ODE45 with a step size of 0.15, the 2×10^{-5} is taken as stability accuracy. For the above three pairs of controlled systems, the number of iterations required to reach the stability under finite-time control and infinite-time control at the accuracy of 2×10^{-5} is shown in Tables 2 and 3. The comparisons data in Table 2 is not prominent due to the small physical parameters of the controlled objects (see Table 1) and the poor smoothness of the ODE45 algorithm used for the solution. However, the MLSs under finite-time control is exactly able to converge to stability. That is, it is a certain consensus that all robots reach finite-time convergence. Under infinite-time control, such consensus is indeterminate.

4.2 Formation consensus under two topology examples

The second part will present the formation performance under the bipartite topology $\mathcal{G}_2$. This part experiment considers the formation of $\mathcal{H}_4$ realized by MLSs under the non-bipartite topology (Figure 1(a)) and the bipartite topology (Figure 1(b)). $\mathcal{H}_4$ represents two concentric forms, positive triangle and positive pentagon.

Under the non-bipartite topology, the formation of 8 robots is shown in Figure 6(a). In Figure 4, the 8 robots are aligned to maintain relative displacement according to the given formation. The MLSs under

Table 2 Iterations required for stabilization under finite time control

Simulation	State	Robot 1	Robot 2	Robot 3	Robot 4	Robot 5	Robot 6	Robot 7	Robot 8
$\mathcal{H}_1$	q_{i1}	238	297	376	8	527	314	362	421
	q_{i2}	404	479	552	335	398	466	256	339
$\mathcal{H}_2$	q_{i1}	352	412	271	331	410	439	246	293
	q_{i2}	287	323	200	449	241	109	189	104
$\mathcal{H}_3$	q_{i1}	281	348	364	232	145	375	457	534
	q_{i2}	226	561	353	131	495	305	359	159

Table 3 Iterations required for stabilization under infinite time control

Simulation	State	Robot 1	Robot 2	Robot 3	Robot 4	Robot 5	Robot 6	Robot 7	Robot 8
$\mathcal{H}_1$	q_{i1}	535	335	425	502	563	639	403	480
	q_{i2}	729	508	872	655	725	498	589	653
$\mathcal{H}_2$	q_{i1}	711	497	277	646	720	475	575	352
	q_{i2}	53	348	438	513	149	260	138	89
$\mathcal{H}_3$	q_{i1}	650	387	459	241	335	415	772	605
	q_{i2}	540	614	402	110	536	329	110	180

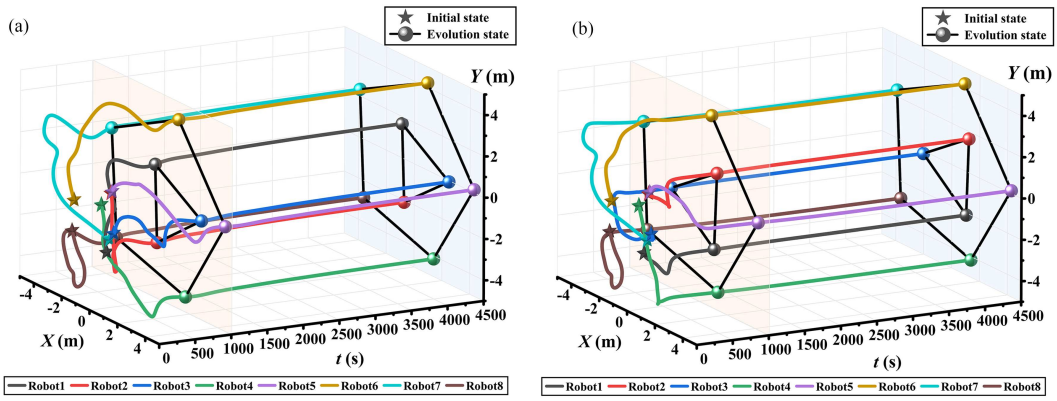

Figure 6 (Color online) Formation consensus of $\mathcal{H}_4$ under two topology examples. (a) $\mathcal{G}_1$: non-bipartite topology; (b) $\mathcal{G}_2$: bipartite topology.

the bipartite topology also complete the formation in Figure 6(b). However, it is noted that, due to the bipartite relationship $\phi_1 = \phi_2 = \phi_3 = -1$, the formation consensus of the robots 1–3 in Figure 6(b) is symmetric with their consensus in Figure 6(a). Figures 7 and 8 show the convergence process of the displacements and velocities in achieving the formation consensus, respectively. For more, the coordinated formation control of MRSs based on Lagrange dynamics under bipartite topology can be found in [29].

4.3 Finite-time tenders tracking with formation

In this part, two sets of tender-tracking examples will be presented for the composite formation of MLSs. The experiments concern the tracking simulations of $\mathcal{J}(t)$ (Eq. (44)) with $\mathcal{H}_4$ as the formation for 8 robots, which are established with the bipartite topology $\mathcal{G}_2$ (Figure 1(b)).

4.3.1 *Tender-B_1 tracking of $\mathcal{J}(t)$ with formation of $\mathcal{H}_4$*

As the tender elements are set to B_1 (see Figure 9(a)), the formation tracking results are given by Figure 10(a). That is, the tracking is required to be performed by robot2 and robot3 with a cooperative relationship within 15 s and by the robot3 and the robot4 with a competitive relationship in 15–30 s. Then, all robots reach the formation. In this case, the responses and convergences of the displacements as well as the velocities of the MLSs are shown in Figures 11(a) and 12(a), respectively.

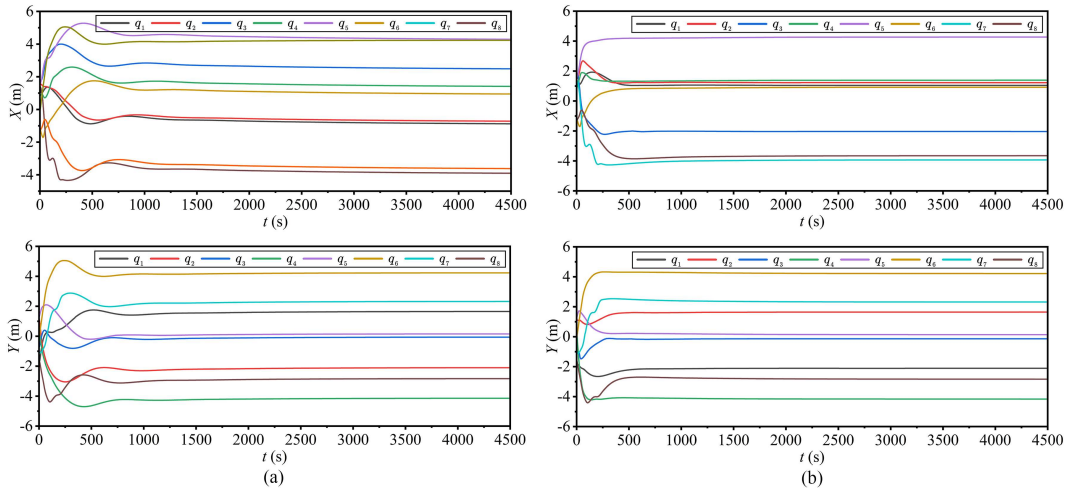

Figure 7 (Color online) Finite-time convergence of the displacements. (a) Formation under $\mathcal{G}_1$; (b) formation under $\mathcal{G}_2$.

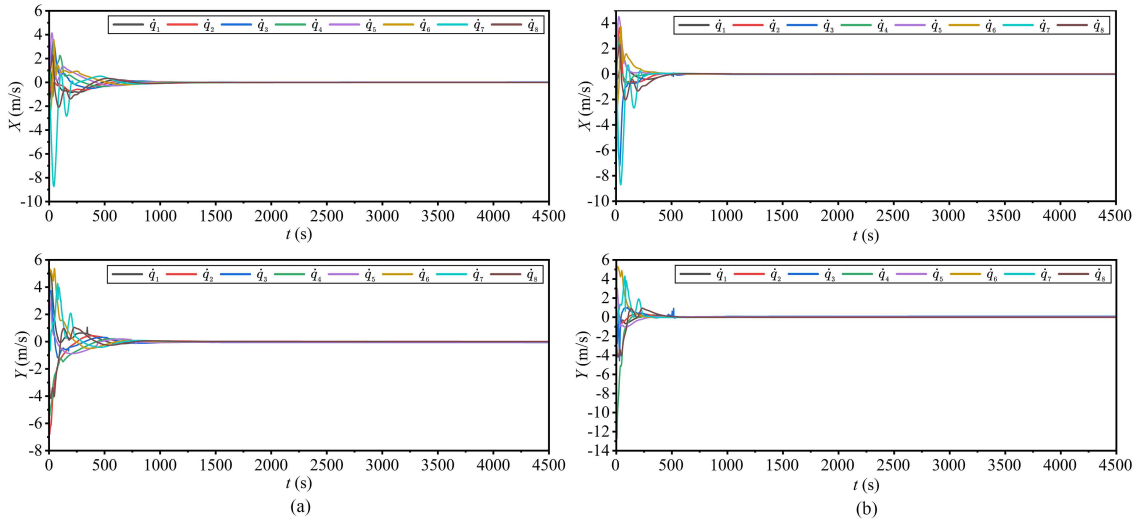

Figure 8 (Color online) Finite-time convergence of the velocities. (a) Formation under $\mathcal{G}_1$; (b) formation under $\mathcal{G}_2$.

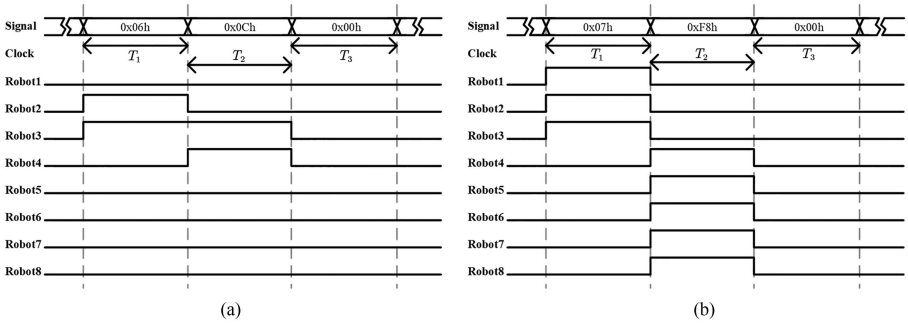

Figure 9 Selected tenders. (a) B_1; (b) B_2.

4.3.2 *Tender-B_2 tracking of $\mathcal{J}(t)$ with formation of $\mathcal{H}_4$*

Based on the bipartite topology $\mathcal{G}_2$, the tender elements are therefore set to B_2 (see Figure 9(b)). That is, the tracking is required to be performed by the robots $\in \{1, 2, 3\}$ within 15 s, by the robots $\in \{4, 5, 6, 7, 8\}$ in 15–35 s. And all robots reach formation in 35–50 s. In this case, the formation tracking results of MLSs are given by Figure 10(b). Figures 11(b) and 12(b) show the responses and convergences of MLSs' displacements as well as the MLSs' velocities.

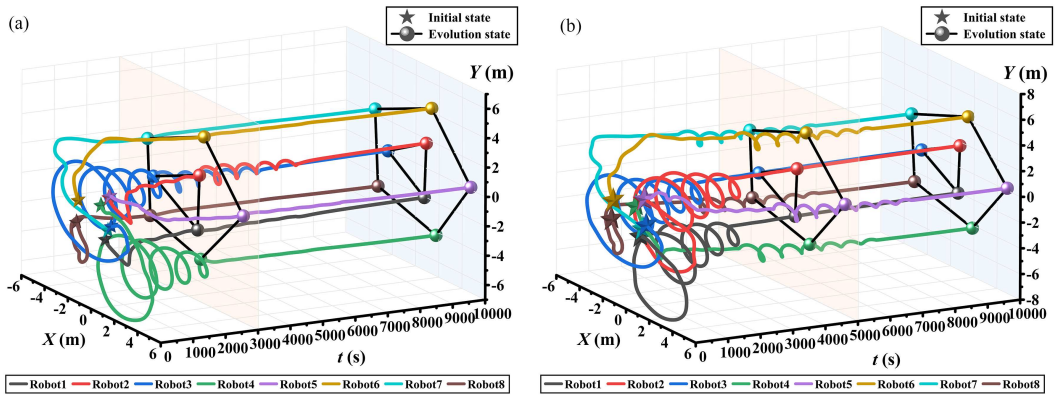

Figure 10 (Color online) Examples of tender-tracking relating to the selected tender. (a) Composite formation of B_1-tracking; (b) composite formation of B_2-tracking.

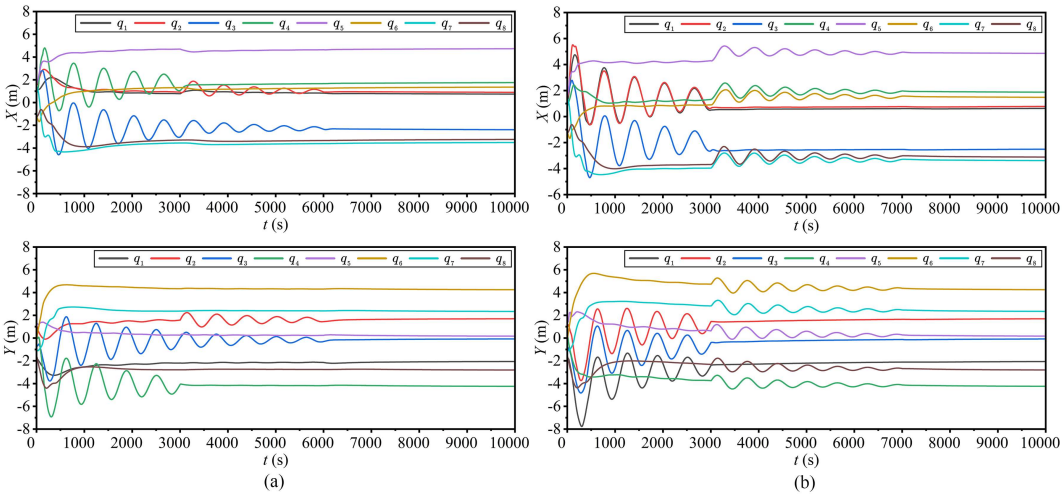

Figure 11 (Color online) Finite-time formation tracking of $(\mathcal{H}_4, \mathcal{J}(t))$ under $\mathcal{G}_2$. Displacements convergence: (a) case of tender-B_1 tracking; (b) case of tender-B_2 tracking.

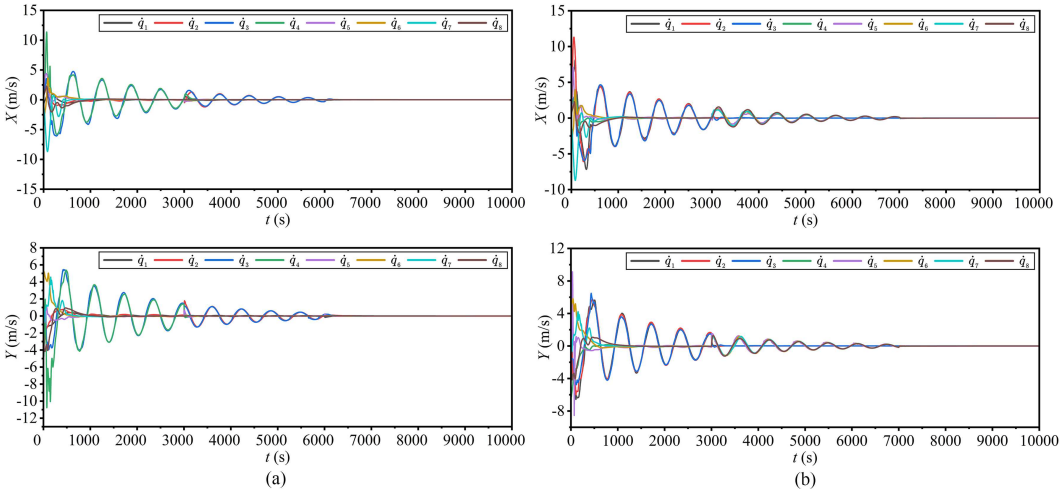

Figure 12 (Color online) Finite-time formation tracking of $(\mathcal{H}_4, \mathcal{J}(t))$ under $\mathcal{G}_2$. Velocities convergence: (a) case of tender-B_1 tracking; (b) case of tender-B_2 tracking.

With the above results, it is concluded as follows.

Remark 6. MLSs perform tracking and formation responses according to tenders and achieve stability with finite-time consensus under control. In case of large global formation errors due to individual track-

ing, MLSs correct the local formation errors through global adjustment to correct the global formation. This, in turn, is the advantage carried by displacement-based formation.

5 Conclusion

In this paper, the work on reaching composite formation of finite-time consensus for nonlinear second-order MRSs was completed. The control protocols for the proposed composite formation problems considered the convergence rates as one controlled variable. Accordingly, the adaptive control protocols based on the coupled sliding variables were given with the consideration of the nonlinear coupling and parametric uncertainty of MLSs. The given coupled-sliding-variable-based protocols were firstly verified in finite-time formation consensus and were further confirmed for the finite-time consensus of tender time-varying tracking. Meanwhile, the experiments of finite-time formation and finite-time composite formation were simulated.

Moreover, the approaches to design finite-time controllers using coupled sliding variables in the paper are worth generalization. Notably, the proposed tender-tracking in the paper can be extended to more flexible CFC problems. More research work is worthwhile, such as combining Radar signals for heterogeneous MRSs' coordination, solving the time-varying formation problems, and dealing with the topology of local time-varying.

Acknowledgements This work was supported by National Natural Science Foundation of China (Grant Nos. 62073209, 61827812, 61991415), Shandong Provincial Natural Science Foundation of China (Grant No. ZR2020KA005), Key Research and Development Project of Shandong Province of China (Grant No. 2021RKY02033).

References

1 Olfati-Saber R, Murray R M. Consensus problems in networks of agents with switching topology and time-delays. IEEE Trans Automat Contr, 2004, 49: 1520–1533
2 Ren W, Beard R W. Consensus seeking in multiagent systems under dynamically changing interaction topologies. IEEE Trans Automat Contr, 2005, 50: 655–661
3 Lu N, Zhou W, Yan H, et al. A two-stage dynamic collision avoidance algorithm for unmanned surface vehicles based on field theory and COLREGs. Ocean Eng, 2022, 259: 111836
4 Venkataraman S T, Gulati S. Control of nonlinear systems using terminal sliding modes. In: Proceedings of American Control Conference, Chicago, 1992, 29. 891–893
5 Bhat S P, Bernstein D S. Finite-time stability of continuous autonomous systems. SIAM J Control Optim, 2000, 38: 751–766
6 Xiao F, Wang L, Chen J, et al. Finite-time formation control for multi-agent systems. Automatica, 2009, 45: 2605–2611
7 Li S, Du H, Lin X. Finite-time consensus algorithm for multi-agent systems with double-integrator dynamics. Automatica, 2011, 47: 1706–1712
8 Zhao Y, Liu Y, Wen G, et al. Distributed finite-time tracking of second-order multi-agent systems: An edge-based approach. IET Control Theor & Appl, 2018, 12: 149–154
9 Li Y, Zhao Y, Liu W, et al. Adaptive fuzzy predefined-time control for third-order heterogeneous vehicular platoon systems with dead zone. IEEE Trans Ind Inf, 2023, 19: 9525–9534
10 Zhou W, Fu J, Yan H, et al. Event-triggered approximate optimal path-following control for unmanned surface vehicles with state constraints. IEEE Trans Neural Netw Learn Syst, 2023, 34: 104–118
11 Wu W, Tong S. Collision-free adaptive fuzzy formation control for stochastic nonlinear multiagent systems. IEEE Trans Syst Man Cybern Syst, 2023, 53: 5454–5465
12 Cui M, Tong S. Event-triggered predefined-time output feedback control for fractional-order nonlinear systems with input saturation. IEEE Trans Fuzzy Syst, 2023, 31: 4397–4409
13 Wu Y, Yang X, Yan H, et al. Adaptive fuzzy event-triggered sliding-mode control for uncertain euler-lagrange systems with performance specifications. IEEE Trans Fuzzy Syst, 2023, 31: 1566–1579
14 Liu J, Zhou J. Distributed impulsive group consensus in second-order multi-agent systems under directed topology. Int J Control, 2015, 88: 910–919
15 Liu J, Ji J, Zhou J, et al. Adaptive group consensus in uncertain networked Euler-Lagrange systems under directed topology. Nonlinear Dyn, 2015, 82: 1145–1157
16 Liu J, Li H, Luo J. Bipartite consensus in networked euler-lagrange systems with uncertain parameters under a cooperation-competition network topology. IEEE Control Syst Lett, 2019, 3: 494–498
17 Roy S, Roy S B, Kar I N. Adaptive-robust control of euler-lagrange systems with linearly parametrizable uncertainty bound. IEEE Trans Contr Syst Technol, 2017, 26: 1842–1850
18 Lu M, Liu L. Leader-following consensus of multiple uncertain Euler-Lagrange systems with unknown dynamic leader. IEEE Trans Automat Contr, 2019, 64: 4167–4173
19 Ge M F, Liu Z W, Wen G, et al. Hierarchical controller-estimator for coordination of networked Euler-Lagrange systems. IEEE Trans Cybern, 2019, 50: 2450–2461
20 Dong Y, Chen Z. Fixed-time synchronization of networked uncertain Euler-Lagrange systems. Automatica, 2022, 146: 110571
21 Yu J, Ji J, Miao Z, et al. Neural network-based region reaching formation control for multi-robot systems in obstacle environment. Neurocomputing, 2019, 333: 11–21
22 Sun Y, Chen L, Qin H, et al. Distributed finite-time coordinated tracking control for multiple Euler-Lagrange systems with input nonlinearity. Nonlinear Dyn, 2019, 95: 2395–2414
23 Zhou P, Chen B M. Formation-containment control of Euler-Lagrange systems of leaders with bounded unknown inputs. IEEE Trans Cybern, 2022, 52: 6342–6353

24 Zhao Y, Duan Z, Wen G. Distributed finite-time tracking of multiple Euler-Lagrange systems without velocity measurements. Int J Robust Nonlinear Control, 2015, 25: 1688–1703
25 Fan Y, Jin Z, Guo B, et al. Finite-time consensus of networked Euler-Lagrange systems via STA-based output feedback. Int J Control Autom Syst, 2022, 20: 2993–3005
26 Altafini C. Consensus problems on networks with antagonistic interactions. IEEE Trans Automat Contr, 2013, 58: 935–946
27 Slotine J J E, Li W. Applied Nonlinear Control. Englewood Cliffs: Prentice-Hall, 1991
28 Hardy G H, Littlewood J E, Pólya G, et al. Inequalities. Cambridge: Cambridge University Press, 1952
29 Ma X, Liu J, Li H, et al. Bidirectional formation-involved consensus for uncertain multi-Lagrange systems under directed signed topology networks. Nonlinear Dyn, 2023, 111: 12197–12212